Probability density field of acoustic emission events
Damage identification in concrete structures

Zhang, Fengqiao; Yang, Yuguang; Naaktgeboren, Marius; Hendriks, Max A.N.

DOI
10.1016/j.conbuildmat.2022.126984

Publication date
2022

Document Version
Final published version

Published in
Construction and Building Materials

Construction and Building Materials 327 (2022) 126984

Contents lists available at ScienceDirect

Construction and Building Materials

journal homepage: www.elsevier.com/locate/conbuildmat

Probability density field of acoustic emission events: Damage identification in concrete structures

Fengqiao Zhang [a,*], Yuguang Yang [a], Marius Naaktgeboren [b], Max A.N. Hendriks [a,c]

[a] Department of Engineering Structures, Delft University of Technology, 2628CN Delft, the Netherlands
[b] Rijkswaterstaat, Ministry of Infrastructure and Water Management, 3526LA Utrecht, the Netherlands
[c] Department of Structural Engineering, Norwegian University of Science and Technology, 7491 Trondheim, Norway

ARTICLE INFO

Keywords:
Probability density function
Acoustic emission source localization
Source localization error
Acoustic emission event density
Damage identification
Concrete structures

ABSTRACT

This paper proposes a new damage identification method, namely, the probability density field of acoustic emission (AE) events. This new method provides a different perspective to deal with the uncertainties in the source localization process. We treat the source location as a random variable, and estimate its probability density field based on a probability density function. The function was found from simulations where various uncertainties were included. The probability of AE events falling in a certain space range is the integral of the probability densities over that range. We apply the new method in a failure test of a full-scale reinforced concrete beam. The resultant probability density field clearly reflects the crack patterns of the specimen and a close relationship with the crack width.

1. Introduction

Damage identification in concrete structures, in many cases, requires the crack location and width [1–4]. These parameters are mostly acquired by displacement measurements like linear variable differential transformer (LVDT), laser distance finder, or digital image correlation (DIC) [5]. The displacement measurements have the advantages of high accuracy, but they can only measure concrete cracking at structural surface. Identification of internal damages is also important. A critical cracking location for structural failure could be inside the concrete element [6,7].

Acoustic emission (AE) is a promising technique to detect internal damages in concrete structures [8,9]. The basic working principle is that sudden changes in concrete, like cracking, will release energy and generate elastic waves. These waves will propagate in the concrete medium and received by AE sensors on the structural surface [10]. The received signals can be used to estimate the source location (which is called source localization [11]), classify the source type (which is called source classification [12]) and determine the damage level of the structure [13]. AE has been widely applied in monitoring concrete structures [14–17]. Among all its capabilities, the scope of this paper is using AE source localization to identify concrete cracking.

AE source localization in concrete structures is influenced by many factors, including the arrival time picking error [18], uncertainty of concrete material properties [19] and sensor locations [20]. These factors can lead to the estimated locations away from the actual locations (which is referred as source localization error) up to 150 mm [20].

To reduce the source localization error, many algorithms have been developed in literature, including using akaike information criterion (AIC) to more accurately pick the arrival time [21] and using variable wave speed models to simulate uncertainty of concrete material properties [22,23]. However, the uncertainties in the localization process cannot be entirely removed. Therefore, some methods quantify the uncertainties and estimate the probability of source location. On estimating the probability, different approaches have been developed [24–26]. Among them, a Bayesian probabilistic method from Schumacher et al. comprehensively includes various uncertainties in the localization process, which are wave velocity, picked arrival time and event time [25]. These parameters are estimated before localization using an inference model. In practice, however, the concrete medium continuously changes due to cracking. New model parameters need to be involved and updated. This is usually time consuming. Even for now, without introducing and updating new parameters, the computational time for one event is reported to be around 50 s. Considering a rapid succession of AE events during concrete cracking, this long computational time is not practical for real-time monitoring, especially in a load

* Corresponding author.
E-mail address: F.Zhang-5@tudelft.nl (F. Zhang).

https://doi.org/10.1016/j.conbuildmat.2022.126984
Received 4 December 2021; Received in revised form 4 February 2022; Accepted 23 February 2022
Available online 28 February 2022

testing.

This paper proposes a new and simplified probabilistic approach, which considers uncertainties from arrival time picking, presence of crack and sensor layouts. For a given AE event obtained by a localization process, we describe the probability of the location of this event in the 1D, 2D or 3D space using a probability density function. The function is found from a simulated source localization process. With more AE events occurring, by simply adding up the probability density field of each AE event, we are able to get the probability density field of all AE events. The probability of the amount of AE events falling in a certain space range is the integral of the probability densities over that range. With the new approach, we can quantify the AE events distribution in a probabilistic manner, considering the uncertainties during the process. This is an important base for further quantifying the local crack width using AE. And, due to its simple calculation, the method costs less time than other more complex probabilistic methods and is applicable for real-time monitoring. The new method is implemented in load testing of a reinforced concrete beam.

2. Probability density field of AE events

The new approach deals with AE events whose locations have been estimated by a source localization process. To estimate the source locations, this paper uses the grid search method [10]. The algorithm estimates the source location at the grid which gives the minimal residual between calculated and measured distance. The residual is

$$r(\mathbf{x}_{g,p}) = \sum_{i=1}^{N-1}\sum_{j=i+1}^{N}\left[\|\mathbf{x}_{g,p}-\mathbf{x}_{r,i}\| - \|\mathbf{x}_{g,p}-\mathbf{x}_{r,j}\| - c\bullet\left(t_{r,i}-t_{r,j}\right)\right]^2, p \in \{1,2,\cdots P\} \quad (1)$$

where, $\mathbf{x}_{g,p}$ is the location of grid point p (g represents 'grid'), $\mathbf{x}_{r,i}$ and $\mathbf{x}_{r,j}$ are the locations of receivers i and j respectively (r represents 'receiver'), $t_{r,i}$ and $t_{r,j}$ are the arrival times at receivers i and j respectively, c is the wave speed which can be measured in a preliminary test [27], P is the number of predefined grid points, and N is the number of sensors.

Other localization methods can also be used, such as those considering a variable velocity distribution [22]. In that case, the estimation of source localization error will need to be adjusted. Readers can do the estimation following the same step as described in Section 3.

As stated before, the estimated source location is not the actual one, due to inevitable source localization errors. The new method considers the errors in a probabilistic manner. Instead of considering the source location as one deterministic point, the new approach evaluates the probability density function of the source location assuming it as a random variable.

The following subsections introduce the new approach by first deriving probability density field of one AE event, then, expanding to more AE events in the measuring time and space range. After derivation, the physical meaning of probability density field of AE events is discussed.

2.1. Single AE event

To estimate the probability of the location of one AE event, a study of source localization error is needed. In this paper, the source localization error is defined as the relative location of the estimated source location to the actual location

$$\Delta = \mathbf{x}_s - \mathbf{x}_g \quad (2)$$

where, $\mathbf{x}_s$ is the actual source location and $\mathbf{x}_g$ is the estimated source location.

The magnitude of source localization error $\|\Delta\|$ is the Euclidian distance between the actual and estimated source locations

$$\|\Delta\| = \sqrt{\sum_{i=1}^{k}\Delta_i^2}, k \in \{1,2,3\} \quad (3)$$

where, k is the dimension of the measuring zone which could be 1D, 2D or 3D and Δ_i is the error component in the i^{th} direction.

We assume that the error component Δ_i follows a normal distribution, with zero mean and standard deviation σ, which is the same for all directions. A same normal distribution ignores the possible anisotropic distribution of the source localization error in concrete structures. The anisotropy could come from the alignment of cracks between the source and the receivers, or from different sensor spacing in different directions. Since this anisotropy is hard to be quantified and may vary from case to case, for a general case, this paper assumes an isotropic source localization error.

Under this assumption, we can determine the probabilistic density function of the source localization error $\mathbf{\Delta}=(\Delta_1,\cdots,\Delta_k)^T$ as

$$f(\Delta) = \frac{1}{\left(\sqrt{2\pi}\right)^k}\frac{1}{\sigma^k}e^{-\|\Delta\|^2/2\sigma^2}, k \in \{1,2,3\} \quad (4)$$

For 1D source localization, the scalar-valued error $\mathbf{\Delta} = \Delta_1$ follows a normal distribution with mean zero and standard deviation σ. For 2D and 3D source localization, the error $\mathbf{\Delta}$ follows a multivariate normal distribution with uncorrelated error components Δ_i, with mean zero and the same standard deviation σ.

With the estimated source location as the origin, we are able to create the probability density at any point $\mathbf{x}$ as

$$f(\mathbf{x},\mathbf{x}_g) = \frac{1}{\left(\sqrt{2\pi}\right)^k}\frac{1}{\sigma^k}e^{-\|\mathbf{x}-\mathbf{x}_g\|^2/2\sigma^2}, k \in \{1,2,3\} \quad (5)$$

where, $\mathbf{x}_g$ is the estimated source location, $\mathbf{x}$ is a random point in the space of k dimensions. The probability density at points in the whole space form the probability density field of the AE event. The integration of probability densities over the whole space equals 1.

Here, an infinite space where the source could be located is considered. However, source localization in concrete structures is clearly bound by the dimension of the concrete structure itself and the measuring zone inside it. This paper neglects the effect from assuming an infinite space in the probability distribution.

Regarding the source localization error magnitude $\|\Delta\|$, since we assume that the error component follows a normal distribution, by definition, the error magnitude can be described by a chi distribution [28]. The standard chi distribution is:

$$\chi(x,k) = \frac{x^{k-1}e^{-x^2/2}}{2^{k/2-1}\Gamma(k/2)}, x \geq 0, k \in \{1,2,3\} \quad (6)$$

where, $\Gamma(k/2)$ is gamma function with $\Gamma(1/2) = \sqrt{\pi}$, $\Gamma(1) = 1$ and $\Gamma(3/2) = \sqrt{\pi}/2$, and $x = \sqrt{\sum_{i=1}^{k}y_i^2}$ where y_i independently follows a standard normal distribution (mean 0 and standard deviation 1).

In our case of source localization, the error component $\Delta_i = y_i\sigma$. Therefore, x is related to the error magnitude $\|\Delta\|$ as

$$x = \sqrt{\sum_{i=1}^{k}y_i^2} = \sqrt{\sum_{i=1}^{k}\left(\frac{\Delta_i}{\sigma}\right)^2} = \frac{1}{\sigma}\sqrt{\sum_{i=1}^{k}\Delta_i^2} = \frac{\|\Delta\|}{\sigma}, k \in \{1,2,3\} \quad (7)$$

Then, the standard chi distribution of x can be transformed into the distribution of error magnitude $\|\Delta\|$

$$g(\|\Delta\|,k) = \chi(x,k)\frac{\partial x(\|\Delta\|)}{\partial\|\Delta\|} = \frac{\chi(x,k)}{\sigma}, x \geq 0, k \in \{1,2,3\} \quad (8)$$

which is written as

$$g(\|\Delta\|,k)=\frac{\|\Delta\|^{k-1}e^{-\|\Delta\|^2/(2\sigma^2)}}{2^{k/2-1}\Gamma(k/2)}\frac{1}{\sigma^k},k\in\{1,2,3\} \tag{9}$$

For 1D source localization, $k=1$, the chi distribution is also known as half-normal distribution; for 2D source localization, $k=2$ leads to a Rayleigh distribution; for 3D source localization, the chi distribution with $k=3$ is Maxwell-Boltzmann distribution. Fig. 1 shows the three distributions at a same standard deviation of the error component σ. A higher degree of freedom k gives a larger expected value of error magnitude. The value of σ is taken as 39 mm, which is found from simulated tests described in Section 3.2.

2.2. Multiple AE events

When more AE events occur during monitoring, the probability density field of each event can be added, resulting in a probability density field of multiple AE events. For all AE events that occur in the measuring time and space range, the probability density at a random location $\mathbf{x}$ is calculated as

$$p_{\mathbf{A}}(\mathbf{x})=\sum_{a\in\mathbf{A}}f(\mathbf{x},\mathbf{x}_{g,a})=\sum_{a\in\mathbf{A}}\frac{1}{\left(\sqrt{2\pi}\right)^k}\frac{1}{\sigma^k}e^{-\|\mathbf{x}-\mathbf{x}_{g,a}\|^2/2\sigma^2},k\in\{1,2,3\} \tag{10}$$

where, $\mathbf{A}$ is a set of all AE events that occurred in the measuring time and space range, $\mathbf{x}_{g,a}$ is the estimated location of event a, and other parameters are defined same as before.

Fig. 2 illustrates the whole approach. The required variables/inputs are the arrival times $\mathbf{t}_r$, the sensor locations $\mathbf{x}_r$, the wave speed c and the standard deviation of the error component σ. The first three inputs are required for a deterministic source localization, and the last one is needed additionally for a probabilistic source localization.

2.3. Physical explanation of probability density field of AE events

A more specific description of 'probability density of AE events' is 'probability density of the location of AE events'. The random variable is 'the location of AE events'. Same as any other variable, its probability density at a point can be interpreted as a relative likelihood that the AE events would locate at that point. In other words, the absolute likelihood of AE events to locate exactly at one point is 0. Comparing the probability density at two different points can indicate how much more likely it is that the AE events would locate at one point compared to the other. For example, Fig. 3a shows the probability density field of (the location of) AE event a_1. Due to source localization error, this event can be estimated at any point in the space with different probability. The probability densities at two points p_1 and p_2 are 75.32 m^{-2} and 12.76 m^{-2} respectively. This indicates that the AE event more likely locates at p_1 than at p_2, which makes sense that p_1 is closer to the actual location than p_2.

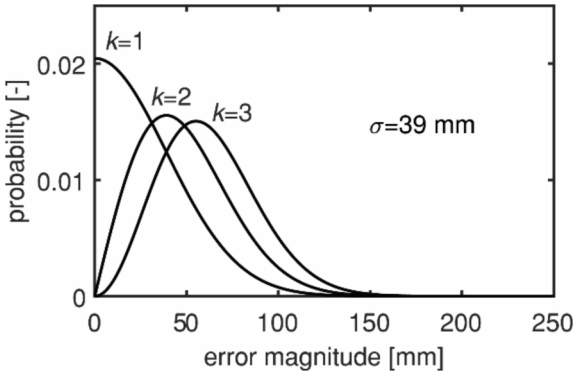

Fig. 1. Probability distribution of error magnitude for k={1,2,3}, with σ = 39 mm.

More precisely, probability density of (the location of) AE events can be used to estimate the probability of AE events falling in a particular space range. The particular space range can be decided freely by the user depending on the purpose of the measurements. For example, when the flexural zone is of more interest, the user could select the flexural zone and calculate the probability in that zone. The probability is then calculated by the integral of the probability densities over that space range. In the same example shown in Fig. 3a, the probability of AE event a_1 located in the area (enclosed by the black frame) is calculated as 0.82. With only one AE event present, the integral over the whole space is 1.

Fig. 3b shows the probability density field of 3 AE events a_1, a_2 and a_3, by cumulating the probability density field of every event. Therefore, the probability density at the same point p_1 increases to 125.27 m^{-2}, and the probability of AE event within the same area (enclosed by the black frame) increases to 1.85. This means that the likelihood that AE events are at point p_1 or within the black frame increases when more AE events occur. The integral over the whole space is the number of AE events (which is 3 in our example).

From the above analysis, probability density of (the location of) AE events at any point is determined by the source localization error distribution, the number and the locations of AE events. Based on the probability density, one can estimate the relative likelihood of AE events located at any point, and estimate the probability of AE events located within a certain space range. Using probability density field of (the location of) AE events is a novel method to quantify AE distribution including uncertainties. In the following sections, the simplified term 'probability density field of AE events' is used.

3. Estimation of source localization error

This section discusses how to obtain the important parameter σ, which is the standard deviation of the error component. The parameter σ is a statistical property, which requires a large amount of tests involving possible uncertainties during source localization. In our previous study [29], we simulated 11,827,200 independent source localization processes, considering arrival time picking error, presence of cracks, and sensor layout. This paper uses the same set of simulations and improves in several aspects, which will be further discussed. Then, we use the simulated magnitude of source localization error and Eq. (9) to determine the parameter σ.

3.1. Description of the simulated source localization process

In this section, we first model a concrete beam and predefine 308 artificial sources in the beam. Then, for each source, we estimate the arrival times considering influence of arrival time picking and presence of crack. Then, based on the influenced arrival times, we calculate the location of each source which can be compared with its real location (which is predefined).

Fig. 4 shows the modelled concrete beam with a relaxed crack. The dimensions of the beam are 3000 mm × 400 mm × 400 mm. Four AE sensors are applied on the surface of the beam. Sensors are arranged in eight different sensor layouts, including two 3D layouts, five 2D layouts, and one 1D layout (Fig. 5). The eight sensor layouts have same maximum sensor spacing. The detection zone is defined as the enclosed zone by the sensors.

The variables of the simulated models are: the maximum sensor spacing $\Delta L_{x,max}$ (see Fig. 4 for the directions), the position and height of the crack (factors α and β in Fig. 4) can be adjusted. When the height of the crack is zero, the model describes the condition without presence of a crack. A total of 24 independent models are built, with $\Delta L_{x,max}$ in the range of 300–1500 mm, α in the range of 0–1, and β in the range of 0–1.

Then, we assume 308 artificial AE sources uniformly distributed in the detection zone (as illustrated in Fig. 6). The wave propagation from the source to the receiver follows the rule that was measured in a previous experiment [27], with a wave speed of 4100 m/s and material

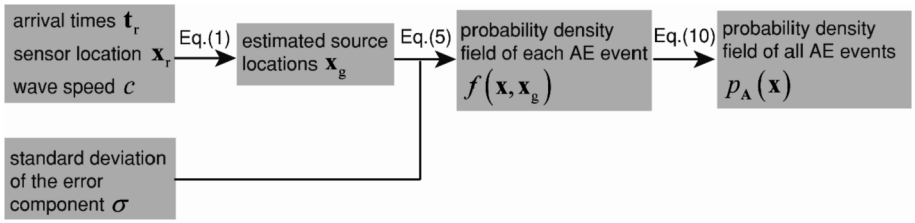

Fig. 2. Derivation of probability density field of AE events.

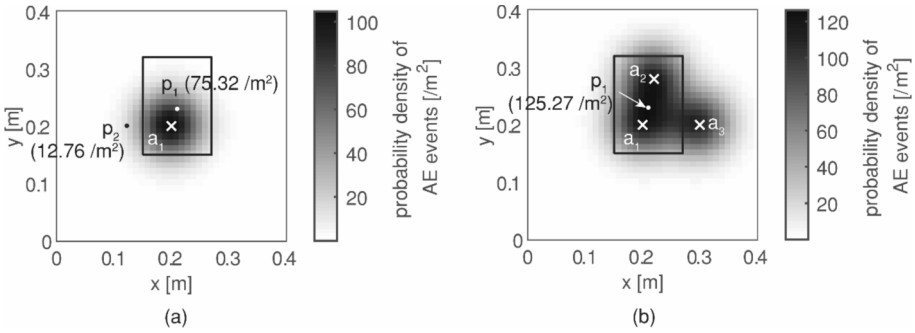

Fig. 3. Illustration of probability density field of (a) one AE event and (b) multiple AE events.

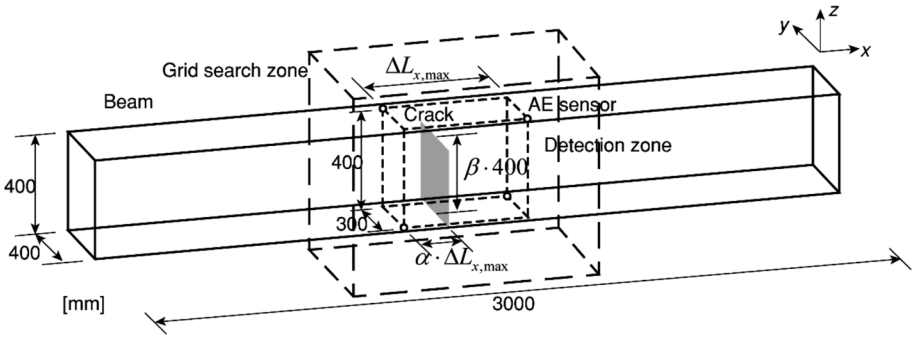

Fig. 4. Configuration of the model.

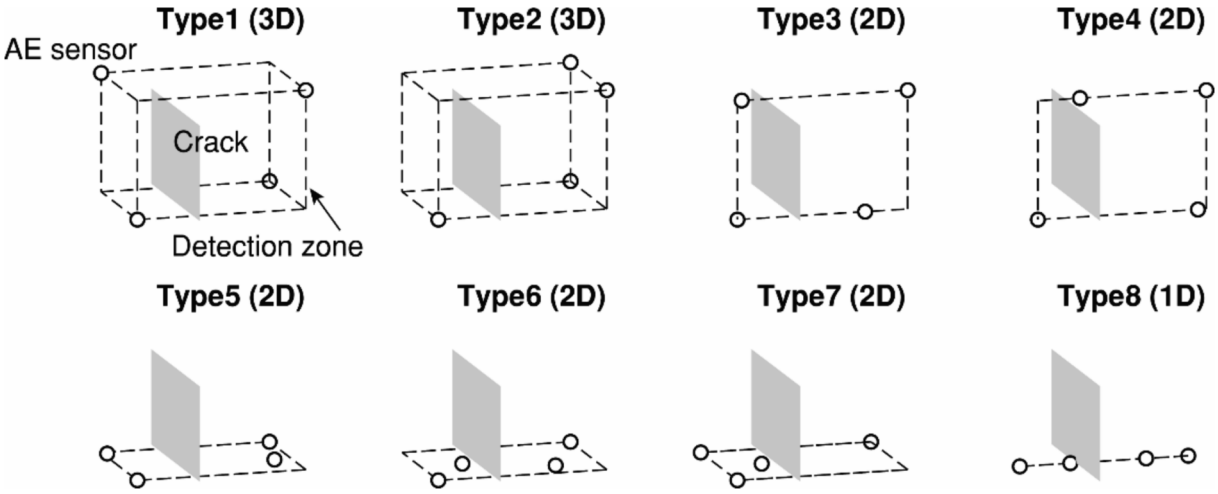

Fig. 5. Sensor layouts, including two 3D layouts, five 2D layouts and one 1D layout.

attenuation factor of 20 dB/m.

The influence of the modelled crack on the arrival time and attenuation is taken into account. According to the measured results [27], the arrival times delay 5 μs and 20 μs when waves propagate parallel and perpendicular to the crack respectively. We consider an elliptical distribution of the wave speed in the crack band of the modelled crack. For

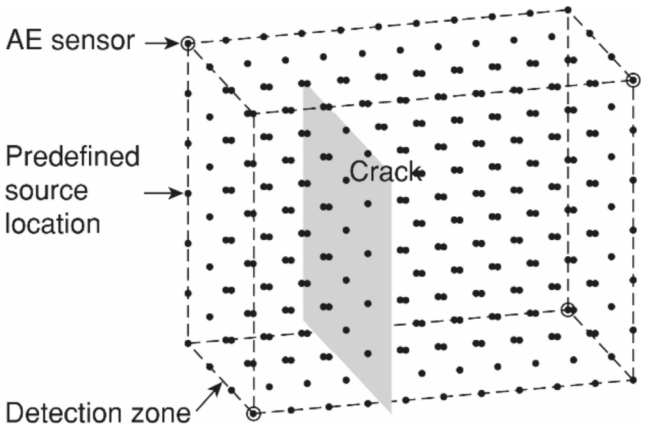

Fig. 6. Predefined source locations uniformly-distributed in the detection zone.

the attenuation, a narrow crack of 0.05 mm was measured to attenuate the signal amplitude by −10 dB, which is considered in this model. In this way, for each source, we can estimate the arrival times at sensors considering the wave propagation in concrete medium and at the modelled crack. This part of simulation is similar to the previous study [29].

In practice, the observed arrival times are also influenced by the arrival time picking method. We evaluate the picking error using signals generated from a lab test on a concrete specimen, which is more representative to our situation. The test setup is described in Section 4.1. During the test, a total number of 29,232 signals from concrete cracking were acquired. For every signal, the arrival time is picked using a fixed threshold of 45 dB. Though the fixed threshold method is the not the most advanced and accurate one, this method is still widely-applied especially in the commercialized monitoring system [30]. To best simulate the practice, we evaluate the arrival time picking error from the fixed threshold method.

The arrival times from the fixed threshold are compared to the real arrival times. Since manual picking of real arrival times is not realistic for such amount of signals and the manual pick may not be accurate either, we use akaike information criterion (AIC) results as reference. AIC picks the arrival times based on iterative statistical analysis [21] which is not influenced by the threshold level and has proven to be substantially more accurate than the fixed threshold method [18]. Fig. 7a shows the comparison and the arrival time picking error

$$\Delta t_p = t_{\text{threshold}} - t_{\text{AIC}} \tag{11}$$

where, $t_{\text{threshold}}$ is the arrival time from the fixed threshold method, t_{AIC} is the arrival time from AIC.

Fig. 7b shows the distribution of the arrival time error in the total 29,232 signals. The error is mostly positive, which means that the result from fixed threshold is later than the AIC result. This is expected, as the fixed threshold value should be larger than the noise level, resulting a later arrival time picking. Although unable to demonstrate the goodness of fit, we assume the (positive) data follows a half-normal distribution with a zero mean, and by comparing with the error distribution, we obtain a standard deviation of 10.5 μs.

In the simulation, we take a random value from the obtained distribution as arrival time picking error for each sensor. In the end, the influenced arrival time is

$$t^* = d/c + \Delta t_{\text{crack}} + \Delta t_p \tag{12}$$

where, d is the distance between predefined source location and the sensor, c is the wave speed, Δt_{crack} is the time delay from the modelled crack, and Δt_p is the arrival time picking error.

With the influenced arrival times, we the use grid search method to calculate back the source location. The grid size is 10 mm. By comparing the calculated source location to the real one (predefined), we can obtain the source localization error.

This procedure is repeated 200 times for the 308 artificial sources in the detection zone of 8 sensor layouts. In the end, a total number of 11,827,200 (24 × 8 × 308 × 200) independent simulated tests are generated. Based on the simulated results, we determine the source localization error distribution in the next section.

3.2. Determination of the error distribution

We first determine the parameter σ in error distribution under the boundary condition that no crack is present between source and receiver ($\beta = 0$).

Fig. 8 shows the counts of the error magnitudes in the eight sensor layouts, with the 95 percentile error magnitude marked. The value of 95 percentile errors reach 165 mm, 156 mm and 90 mm for 3D, 2D and 1D respectively. Within 3D (or 2D) layouts, the variation among different sensor layouts is not large, because the maximum sensor spacing is equal. When the maximum sensor spacing increases to 1 m, the source localization error magnitude gets significantly larger due to absence of direct waves after attenuation. This part of results are not shown in this paper, but can be found in the previous study [29].

As discussed before, we assume that the error magnitude follows a chi distribution described by Eq.(9), in which the shape depends on the dimension k. In the presented study, with the same boundary conditions, we assume that all the simulated results follow chi distributions with a same σ. We normalize the counts of error magnitude in Fig. 8 by scaling the vertical axes. Then, we calculate the residual between the normalized data and the probability density function of chi distribution in each

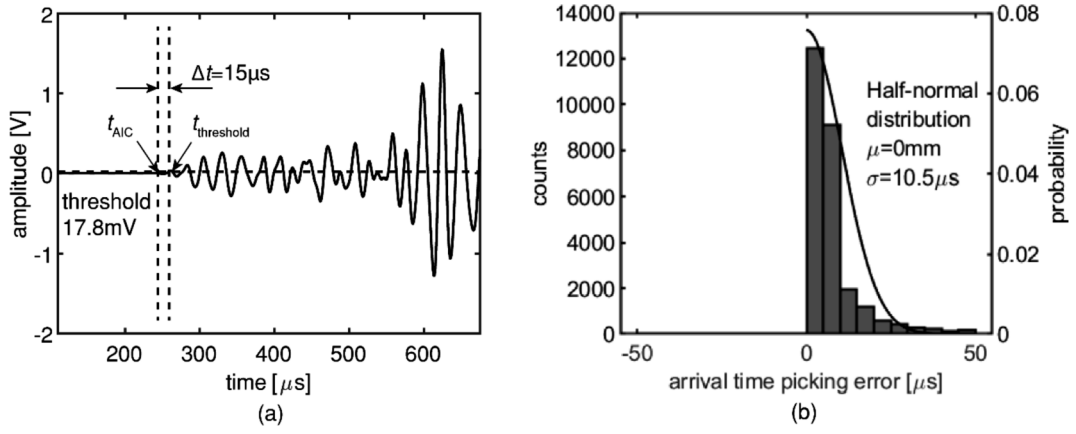

Fig. 7. Arrival time picking error using fixed threshold method compared to AIC results: (a) an example and (b) results of the statistical analysis.

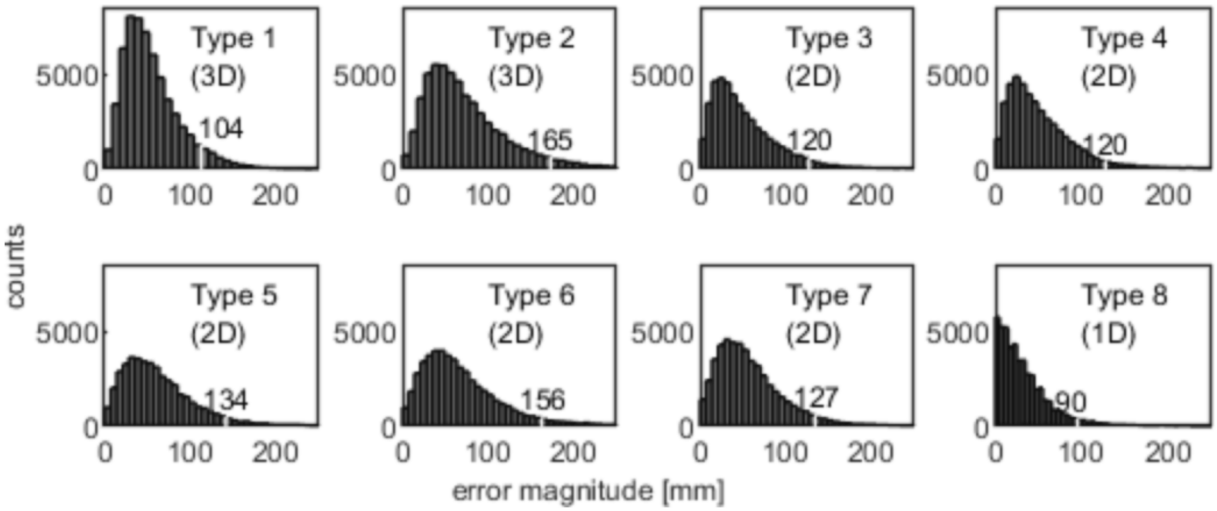

Fig. 8. Counts of the error magnitude in the eight sensor layouts when no crack presents, with the 95 percentile error magnitude marked. (Type 1–2 are 3D layouts, Type 3–7 are 2D layouts, and Type 8 is a 1D layout [29]. All the types had a maximum sensor spacing of 500 mm).

sensor layout. The best-fit probability density functions are based on the single σ value that gives the least sum of residuals of all the sensor layouts. To weigh the residuals of 1D, 2D and 3D equally, we take different weight factors: the two 3D layouts each has a weight factor of 0.5 (=1/2), the five 2D layouts each has a weight factor of 0.2 (=1/5), and the one 1D layout has a weight factor of 1.

From this procedure, the resulting standard deviation of error component σ is 39 mm. Fig. 9 shows the normalized data and the fitted curves, with the 95 percentile error magnitudes marked. The goodness of fit is hard to be improved since we assume a constant parameter σ for every sensor layout type. This paper neglects the effect from sensor layout types as long as they have same maximum sensor spacing. Study on this effect requires more tests on different types of sensor layouts.

For other conditions with a crack between source and receiver, the obtained σ is related to the crack height (Fig. 10a). With increasing crack height, σ increases from 39 mm to 55 mm. The maximum value is obtained when the crack cuts through the measurement volume. Fig. 10b explains this observation. We define a free zone, where the direct ray paths from sources to the receivers do not go through the crack. For sources in this free zone, the source localization is not influenced by presence of the crack. For sources outside the free zone, at least one of the direct ray paths will go through the crack. The crack will delay the arrival time, resulting in large source localization error. When the crack height increases, the volume of free zone is reduced. More percentage of sources will be located with the influence from the crack, giving larger overall source localization error. This explains why the standard deviation of the error component σ increased with crack height.

Table 1 lists the resulting values for σ in conditions of different crack heights, with the 95 percentile error magnitudes for 3D, 2D and 1D layouts. When the concrete in a sensor grid was not previously cracked, condition of zero crack height ($\beta = 0$) applies. When concrete was cracked in a sensor grid, condition of $\beta = 1$ is suggested. This considers the worst scenario when the crack height is not available. When the cracking condition is unknown, one may use $\sigma = 55$ mm for a general case. It should be noticed that the suggested values of σ apply when the direct waves can be received after attenuation.

4. Application in a failure test of a reinforced concrete beam

This section demonstrates the new approach in a failure test of a reinforced concrete beam. The test, named as I123A, was from a series of tests on full-scale reinforced concrete beams [31].

4.1. Test setup

The reinforced concrete beam has dimensions of 10000 mm × 300 mm × 1200 mm (Fig. 11a). The concrete nominal compressive strength is 65 MPa. It is reinforced by 8Ø25 plain bars in two layers at the bottom. The concrete cover is 25 mm.

The beam was loaded under point load at 3 m away from one support (Fig. 11a and b). Five load levels were applied (level 1–5), each containing three cycles (Fig. 12a). The beam failed in shear at 300 kN (in the second cycle of load level 5). Four major flexural cracks (CR1-CR4) developed sequentially from the load position to the support. Fig. 12b

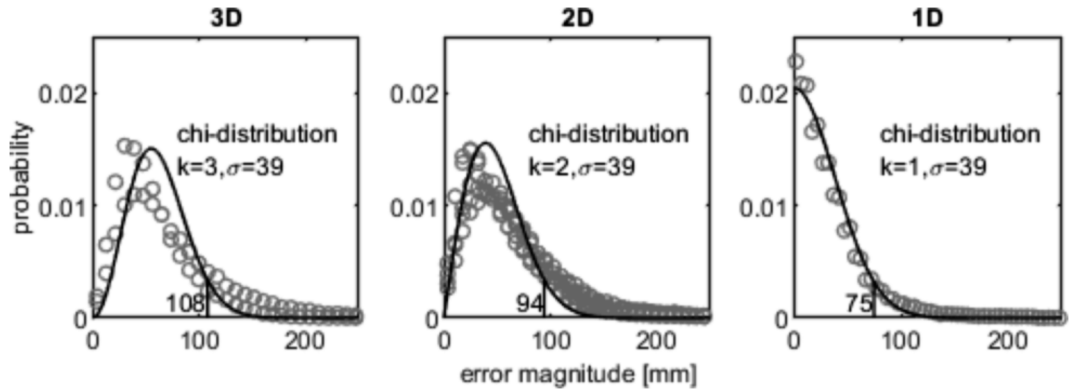

Fig. 9. Probability distribution of the error magnitude when no crack is present, with the 95 percentile error magnitude marked.

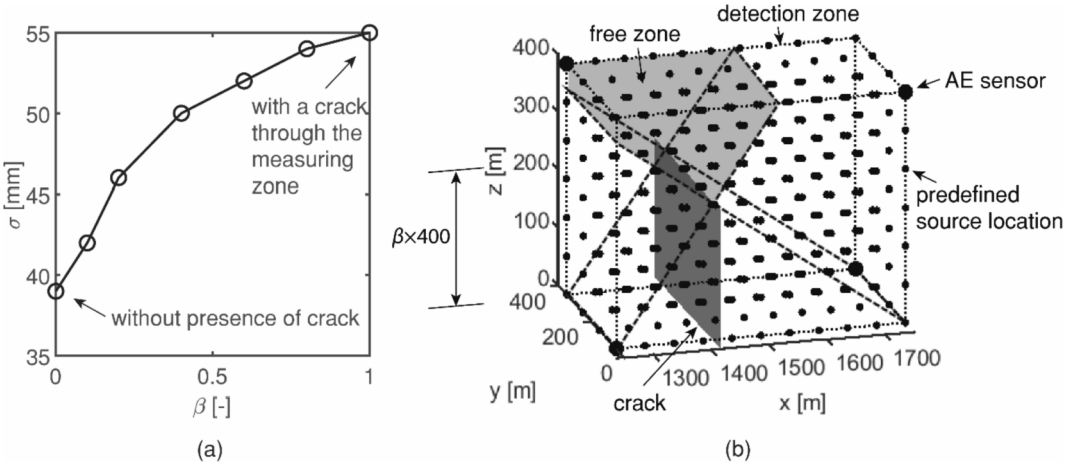

Fig. 10. (a) Standard deviation of the error component in conditions with different crack heights, and (b) illustration of the free zone in source localization with a crack.

Table 1
Summary of standard deviation of error component σ and 95 percentile error magnitude, in conditions of different crack heights.

Condition		Uncracked in a sensor grid	Cracked in a sensor grid					
Crack height factor β		0	0.1	0.2	0.4	0.6	0.8	1
Standard deviation of error component σ [mm]		39	42	46	50	52	54	55
95 percentile error magnitude [mm]	3D	108	116	128	139	144	150	153
	2D	94	102	112	121	126	131	134
	1D	75	81	89	97	101	105	107

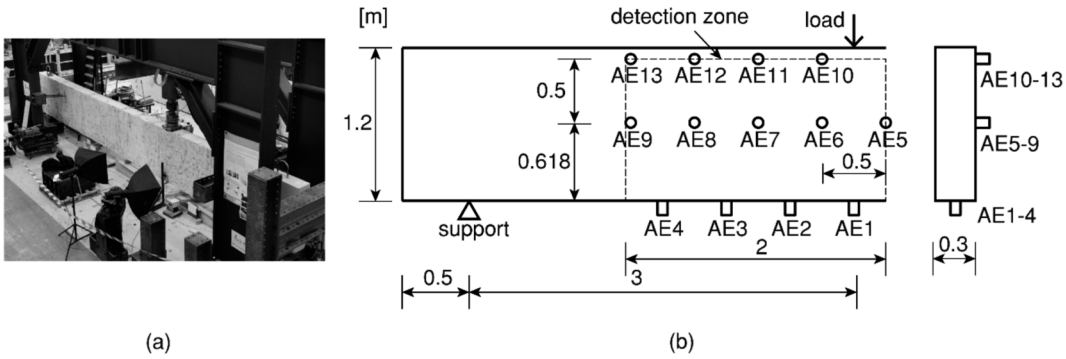

Fig. 11. Test setup: (a) an overview (photo is taken on the DIC side), and (b) beam configuration, load position, one support position, and AE sensor layout.

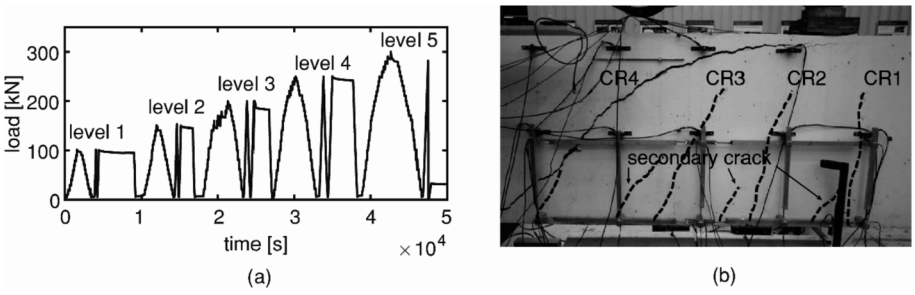

Fig. 12. (a) Loading history and (b) crack patterns at failure.

shows the crack patterns at failure.

Thirteen AE sensors (R6I with central frequency 60 kHz) were installed on the surface of the beam, with nine on one side surface and four on the centroid line of the bottom surface. Fig. 11b shows the sensor layout. The sensor spacing was determined considering the following aspects:

(1) The direct waves should be received by at least three sensors after attenuation. The attenuation property was measured in a preliminary test [27]. After 1 m, the direct wave amplitude reduced 60 dB. For a source signal of 100 dB and noise level of 40 dB, the direct waves could not be detected after 1 m. This test considered 1 m as the maximum allowable sensor spacing. Moreover, by limiting the sensor spacing that the direct waves can be detected after attenuation, the picked first arrivals for source localization would be most-likely from the direct waves, instead of the later-arrived reflections by the structural boundary. In this way, we limit the influence of the reflections on source localization.
(2) Only one crack can be present between two adjacent sensors. On locating AE events from that single crack, no other crack are presents between the source and receiver. In this way, the influence of the presence of cracks was eliminated. Therefore, the sensor spacing should be smaller than the estimated crack spacing. In our experiments, the crack spacing was estimated to be around 0.6 m [32].

Based on these, the sensor spacing in longitudinal direction was set to be 0.5 m, and in height direction maximum 0.618 m.

For calibration, digital image correlation (DIC) measurement was applied on the other side of the beam (Fig. 11a) [33]. Since the beam width was small compared to the length and height, the crack patterns and openings on both sides of the beam were considered comparable.

4.2. Probability density field of AE events

We applied the probabilistic approach for source localization as outlined in Fig. 2 in the beam test. We first estimated the source location using the grid search method. The grid size was 10 mm. The arrival times were picked using the fixed threshold method with threshold value of 45 dB. We applied 2D source localization.

Fig. 13a shows the source localization results accumulated from 0 until 200 kN (without unloading parts). We detected two cracks CR1 and CR2 (numbered in Fig. 12b). Due to the source localization error, the results were scattered. Furthermore, we cannot quantify the AE distribution from this plot.

The next step was to calculate the probability density field of one AE event. From the derivations in Section 2, an important factor is the standard deviation of the source localization error component σ. Since the conditions of the test were in line with the simulation presented in section 3.2 (concrete was not cracked previously, $\beta = 0$), the parameter σ = 39 mm from Table 1 was directly applied. Fig. 13b shows the probability density field of an AE event which was estimated at (2.48,0.35) m.

In the last step, we added up the probability density field of each AE event from 0 to 200 kN and obtained the probability density field of all AE events (Fig. 13c). Comparing to the normal source localization results in Fig. 13a, cracks were more clearly illustrated (even the secondary crack in Fig. 12b can be distinguished).

We took a few points along the crack from the crack tip to the bottom (p_1-p_7). Fig. 13d compares the probability density of AE events and local crack width from DIC at these points. From p_1-p_4 and p_7, we found a proportional relationship between the probability density of AE events and local crack opening. It seems hard to explain why p_5-p_6 had less AE activities with larger crack width. We are now performing further studies to relate the probability density of AE events and the local crack widths.

Following the same procedure, we calculated the probability density field of AE events from 0 to 250 kN (Fig. 14a) and from 0 to 300 kN (Fig. 14b). In both cases, AE during unloading were excluded. At 250 kN, CR3 was detected. At 300 kN (which was close to failure), we acquired a vast amount of AE events along CR4: probability density of AE events reached 50000 m^{-2}, much larger than the value at the previous load level (around 12000 m^{-2}). This was possibly due to more AE events from crack sliding (shear displacement) before failure. This met with the expectation that shear displacement at the critical crack triggered the shear failure [1].

It should be noted that in the bottom part of the beam, near the reinforcements, multiple cracks are present between two adjacent sensors. The error distribution should then have a larger standard deviation σ than the applied 39 mm for other parts, resulting in a more smeared distribution. In this work, we did not consider the spatial variation of the

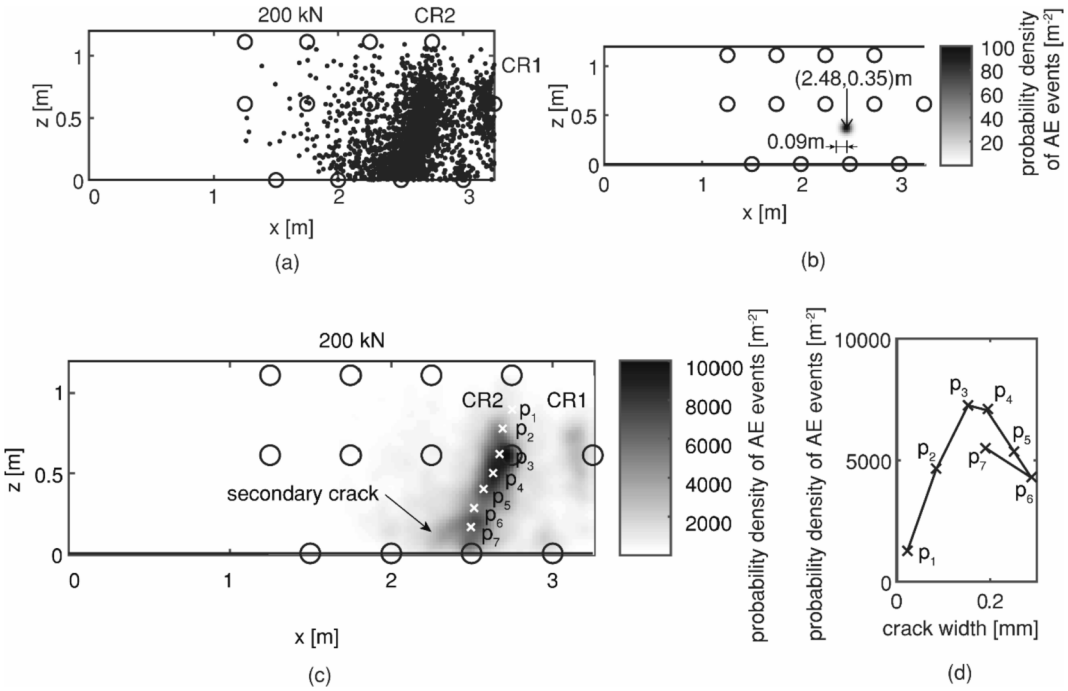

Fig. 13. From 0 to 200 kN (without unloading parts): (a) estimated source locations, (b) probability density field of an AE event at (2.48,0.35) m, (c) probability density field of all AE events, and (d) probability densities at points p_1-p_7 along the crack CR2.

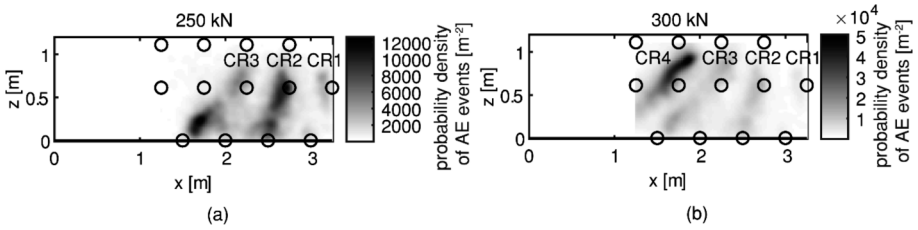

Fig. 14. Probability density field of AE events: (a) from 0 to 250 kN and (b) from 0 to 300 kN, both without unloading parts.

standard deviation.

Moreover, the probability density field can be updated in real time when new AE events occur. In the demonstration, for a single AE event, the total computational time including calculation and visualization was around 0.12 s. This is a significant reduction compared to the more complex probabilistic methods (which was around 50 s per AE event [25]).

This application shows the benefits of probability density field of AE events in damage identification. Firstly, it allows the users to consider the inevitable uncertainties during the localization process, such as arrival time picking error and presence of crack. Secondly, the probability density quantifies the distribution of AE events. And, by comparing the test results, the probability density of AE events can better identify the localised cracking. Even smaller cracks (like the secondary crack), whose AE events are easily masked by the vast amount of AE of a major crack, can be distinguished. Thirdly, this method uses simple calculation that can be applied in real time without much time consuming. Moreover, the probability density of AE events is closely related to the crack width. Exploring the relationship is an on-going work.

5. Recommendations for application in engineering practice

To implement the probability density field of AE events in practice, some remarks are addressed:

- On designing the sensor spacing, two aspects need to be considered. First, the sensor spacing should allow the direct waves being detected by sufficient number of sensors after attenuation. Here, a preliminary measurement on wave attenuation is needed. Second, the sensor spacing is suggested to be smaller than the expected crack spacing. In this way, it is likely that only the crack which generates AE sources is present between two sensors and no other cracks are present between the source and the receiver. This consideration limits the influence from presence of crack.
- This paper uses the grid search method to estimate the source locations. Other localization methods can also be used, such as those considering a variable velocity distribution [22]. A different localization method may provide different source localization errors. Therefore, the standard deviation of error component σ needs to be adjusted correspondingly.
- The influential factor, arrival time picking error, need to be updated if different arrival time picking methods are used. Once the arrival time picking error is determined for a specific test setup, it is suggested to run a similar simulation to get the standard deviation of the error component.
- For the studies that only require the crack patterns, one can directly use the distribution proposed in this paper, without running the simulations.
- For real time monitoring, the probability density field of AE events can be updated at every new AE event.

6. Conclusion and further study

This paper proposes a simple probabilistic method to identify damages in concrete structures, which considers the source localization error. Unlike the conventional source localization methods that aim to accurately estimate the source location, this method provides the probability density of the location of AE events. A key parameter is the standard deviation of error component σ. This paper demonstrates how to determine this parameter from simulated tests. With the key parameter known, we are able to determine the probability density field of AE events. The integral of probability density over a certain space range indicates the probability of AE events located in that space range.

The proposed method has been applied in a reinforced concrete beam. The application shows many benefits of this method. First, the source localization errors are included in a probabilistic manner. Second, the probabilistic approach can provide a clearer crack pattern compared to conventional source localization. Third, the new method is efficient in computational time, thus can perform real time monitoring. Moreover, the probability density of AE events is closely related to the local crack width.

For future studies, the uncertainties that may influence the parameter σ need to be further elaborated, such as different types of sensor layouts. Moreover, it is valuable to further study the relationship between the probability density of AE events and the local crack width (which is on-going).

Funding

This research was funded by Rijkswaterstaat, Ministry of Infrastructure and Water Management.

CRediT authorship contribution statement

Fengqiao Zhang: Conceptualization, Methodology, Software, Validation, Formal analysis, Investigation, Data curation, Visualization, Writing – original draft. **Yuguang Yang:** Conceptualization, Methodology, Resources, Supervision, Project administration, Funding acquisition, Writing – review & editing. **Marius Naaktgeboren:** Resources, Supervision, Funding acquisition. **Max A.N. Hendriks:** Conceptualization, Methodology, Resources, Supervision, Project administration, Funding acquisition, Writing – review & editing.

Declaration of Competing Interest

The authors declare that they have no known competing financial interests or personal relationships that could have appeared to influence the work reported in this paper.

References

[1] Y. Yang, J. den Uijl, J. Walraven, Critical shear displacement theory: on the way to extending the scope of shear design and assessment for members without shear reinforcement, Structural Concrete 17 (5) (2016) 790–798.
[2] Y. Yang, et al., *Calibration of the shear stop criteria based on crack kinematics of reinforced concrete beams without shear reinforcement*, in *fib Congress*, Melbourne, Australia, 2018.
[3] Deutscher Ausschuss fur Stahlbeton 7 (2000).
[4] R.J. Frosch, Another look at cracking and crack control in reinforced concrete, Structural Journal 96 (3) (1999) 437–442.

[5] Zarate Garnica, G., et al., *Monitoring structural responses during proof load testing of reinforced concrete bridges: A review*, in *Tenth International Conference on Bridge Maintenance, Safety and Management (IABMAS 2020)*. 2021: online.
[6] N.V. Tue, W. Theiler, N.D. Tung, Schubverhalten von Biegebauteilen ohne Querkraftbewehrung, Beton- Stahlbetonbau 109 (10) (2014) 666–677.
[7] A. Muttoni M. Fernández Ruiz Shear strength of members without transverse reinforcement as function of critical shear crack width. 105 2 2008 pp. 163–172-163-172.
[8] *fib*, *Monitoring and safety evaluation of existing concrete structures*. *fib* bulletin. Vol. 22. 2003: Elsener and Böhni. 297.
[9] M. Ohtsu, The history and development of acoustic emission in concrete engineering, Mag. Concr. Res. 48 (177) (1996) 321–330.
[10] C. Grosse, and M, Basics for Research-Applications in Civil Engineering, Ohtsu, Acoustic emission testing, 2008, pp. 1–404.
[11] T. Kundu, Acoustic source localization, Ultrasonics 54 (1) (2014) 25–38.
[12] M. Ohtsu, Recommendation of RILEM TC 212-ACD: Acoustic emission and related NDE techniques for crack detection and damage evaluation in concrete: Test method for classification of active cracks in concrete structures by acoustic emission, Mater. Struct. 43 (9) (2010) 1187–1189.
[13] M. Ohtsu, Recommendation of RILEM TC 212-ACD: Acoustic emission and related NDE techniques for crack detection and damage evaluation in concrete: Test method for damage qualification of reinforced concrete beams by acoustic emission, Mater. Struct. 43 (9) (2010) 1183–1186.
[14] A. Carpinteri, G. Lacidogna, G. Niccolini, Damage analysis of reinforced concrete buildings by the acoustic emission technique, Structural Control and Health Monitoring 18 (6) (2011) 660–673.
[15] C. Van Steen et al. On-site inspection of a reinforced concrete structure deteriorated due to corrosion by means of acoustic emission and other techniques 2018 2018: Edinburgh, Scotland.
[16] F. Zhang, G.I. Zarate Garnica, Y. Yang, E. Lantsoght, H. Sliedrecht, Monitoring Shear Behavior of Prestressed Concrete Bridge Girders Using Acoustic Emission and Digital Image Correlation, Sensors 20 (19) (2020) 5622, https://doi.org/10.3390/s20195622.
[17] I. Bayane, E. Brühwiler, Structural condition assessment of reinforced-concrete bridges based on acoustic emission and strain measurements, Journal of Civil Structural Health Monitoring 10 (5) (2020) 1037–1055.
[18] B. Schechinger, T. Vogel, Acoustic emission for monitoring a reinforced concrete beam subject to four-point-bending, Constr. Build. Mater. 21 (3) (2007) 483–490.
[19] E. Tsangouri, G. Karaiskos, A. Deraemaeker, D. Van Hemelrijck, D. Aggelis, Assessment of Acoustic Emission localization accuracy on damaged and healed concrete, Constr. Build. Mater. 129 (2016) 163–171.
[20] Zhang, F., *Evaluation of Acoustic Emission Monitoring of Existing Concrete Structures*, in *Civil Engineering and Geosciences*. 2017, Delft University of Technology: Delft, the Netherlands.
[21] J.H. Kurz, C.U. Grosse, H.-W. Reinhardt, Strategies for reliable automatic onset time picking of acoustic emissions and of ultrasound signals in concrete, Ultrasonics 43 (7) (2005) 538–546.
[22] Gollob, S., *Source localization of acoustic emissions using multi-segment paths based on a heterogeneous velocity model in structural concrete*. 2017, ETH Zürich.
[23] T. Nishida et al. Damage Evaluation of RC Bridge Deck under Wheel Loading Test by Means of AE Tomography Journal of Acoustic Emission 34 2017 p. S26+.
[24] E. Dehghan Niri, S. Salamone, A probabilistic framework for acoustic emission source localization in plate-like structures, Smart Mater. Struct. 21 (3) (2012) 035009, https://doi.org/10.1088/0964-1726/21/3/035009.
[25] T. Schumacher, D. Straub, C. Higgins, Toward a probabilistic acoustic emission source location algorithm: A Bayesian approach, J. Sound Vib. 331 (19) (2012) 4233–4245.
[26] M.R. Jones, et al., A Bayesian methodology for localising acoustic emission sources in complex structures, Mech. Syst. Sig. Process. 163 (2022), 108143.
[27] L. Pahlavan, F. Zhang, G. Blacquière, Y. Yang, D. Hordijk, Interaction of ultrasonic waves with partially-closed cracks in concrete structures, Constr. Build. Mater. 167 (2018) 899–906.
[28] Abell, M.L.L., et al., *Statistics with Mathematica*. 1999: Elsevier Science.
[29] F. Zhang, L. Pahlavan, Y. Yang, Evaluation of acoustic emission source localization accuracy in concrete structures, Structural Health Monitoring 19 (6) (2020) 2063–2074.
[30] MISTRAS, *AEwin SOFTWARE, Installation, Operation and User's Reference Manual*. 2011, Products & Systems Division: Princeton Junction, NJ, USA.
[31] Yang, Y., *Shear behaviour of deep RC slab strips (beams) with low reinforcement ratio*, in *Stevin Report*. 2020, Delft University of Technology: Delft, the Netherlands.
[32] Y. Yang, Shear Behaviour of Reinforced Concrete Members without Shear Reinforcement, Delft University of Technology:, Delft, the Netherlands, 2014.
[33] G. Zarate Garnica, *Analysis of shear transfer mechanisms in concrete members without shear reinforcement based on kinematic measurements*, in *Structural Enigneering*, Delft University of Technology, Delft, 2018.